SRSF3 and HNRNPH1 regulate alternative splicing of PRMT5 induced by ionizing radiation in hepatocellular carcinoma

Chaowei Wen
Wenzhou Medical University
Zhujun Tian
Wenzhou Medical University
Lan Li
Wenzhou Medical University
Shugen Qu
Wenzhou Medical University
Tongke Chen
Wenzhou Medical University
Zhenzhen Liang
Wenzhou Medical University
Huajian Chen
Wenzhou Medical University
Yimeng Ying
Wenzhou Medical University
Jichen Dai
Wenzhou Medical University
Ping Li
Wenzhou Medical University
Yi Liu
Wenzhou Medical University
Mengke Li
Wenzhou Medical University
Shumei Ma
Wenzhou Medical University
Xiaodong Liu (liuxd2014@126.com)
Wenzhou Medical University

Research Article

Keywords: ionizing radiation, PRMT5-ISO5, alternative splicing, SRSF3, HNRNPH1, spontaneous HCC

Posted Date: April 15th, 2022

DOI: https://doi.org/10.21203/rs.3.rs-1533802/v1

Abstract

Background

Aberrant splice variants play different roles in the formation of tumors. We observed the splice isoform of Protein arginine methyltransferase 5 (*PRMT5-ISO5*) increases in HCC patients undergoing stereotactic body radiotherapy, which is associated with improvement of poor prognosis. However, the mechanism of alternative splicing of *PRMT5-ISO5* induced by ionizing radiation (IR) is still unclear.

Methods

The transcriptional changes of *PRMT5-ISO5* induced by IR were validated by reverse transcription quantitative polymerase chain reaction (RT-qPCR) assay. Bioinformatic analyses were performed to identify potential splicing factors involved in regulating *PRMT5* splicing. Small interferring RNA and overexpressing plasmids for SRSF3 and HNRNPH1 were introduced into HCC cell lines, followed by in vitro functional experiments in regulating *PRMT5* splicing by RT-qPCR, western blot and RNA-immunoprecipitation assay in vitro. The roles of IR-induced *PRMT5-ISO5* and hepatocyte-specific *Prmt5* knockout on HCC progression were evaluated in vivo.

Results

we indicated IR could induce *PRMT5-ISO5* transcript in HCC cells by virtue of splicing factors SRSF3 and HNRNPH1. Mechanistically, HNRNPH1 silencing resulted in the decrease *of PRMT5-ISO5* while SRSF3 silencing led to the increase of *PRMT5-ISO5*. In addition, both SRSF3 and HNRNPH1 bound to *PRMT5* precursor mRNA on the region around 3' splicing site of intron 2 and alternative 3’ splicing site on exon 4, leading to their opposite functions on regulating *PRMT5* splicing. In vivo, the increase of *PRMT5-ISO5* induced by IR led to tumor regression, and liver-specific *Prmt5* depletion decelerated the progression of Akt/N-Ras-derived spontaneous HCC.

Conclusion

Our study not only provides mechanistic views that IR-induced SRSF3 downregulation leads to the imbalance of SRSF3 and HNRNPH1 in regulating *PRMT5-ISO5* transcript, but also indicates a potential radiotherapeutic of *PRMT5-ISO5* in HCC formation since liver-specific *Prmt5* knockout inhibits spontaneous HCC tumorigenesis.

Background

Protein arginine methyltransferase 5 (PRMT5), a member of the type II protein arginine methyltransferases, has been confirmed to overexpress in solid tumors and hematological tumors. The

abnormal expression of PRMT5 is associated with poor prognosis [1–4]. PRMT5 catalyzes both monomethylated arginine and symmetric dimethylarginine, either regulating transcription of target genes or post-translationally modulating their functions [5]. For now, no inhibitor targeted to PRMT5 is approved for marketing, though some of them (GSK3326595, JNJ64619178, and PF-06939999) have entered clinical trials for multiple cancers. More effective treatment strategies have been evaluated for targeted therapy combined with PRMT5, such as anti-PD-1 immune checkpoint therapies and chemo-radiotherapy [6–7].

Considering that alternative splicing (AS) concerns up to 95% of human genes, aberrant AS is suggested to be added to the growing list of cancer hallmarks [8–9]. AS can be regulated by cis-elements and the subsequent recruitment of splicing factors. The mutations of cis-elements, as well as the alteration of expression level and activity of splicing factors may lead to AS dysregulation in cancers [10]. The disturbed expression of SR and hnRNP proteins in cancers impairs the function of target apoptotic genes through extrinsic and intrinsic pathways. For instance, SRSF1 and hnRNP A1 promote anti-apoptotic splice isoforms of Bcl-x and Mcl-1, leading to programmed cell death fading in chronic myeloid leukemia and bread cancer [11]. Aberrant expression of SRSF1 and hnRNP K can contribute to the insensitivity of pancreatic and liver cancers response to chemotherapy.

PRMT5, as a prognosis biomarker of various cancers including hepatocellular carcinoma (HCC) [7], has been identified to generate different transcripts which may act unequal biological activities. The canonical transcript *PRMT5* isoform a (NM_006109.5, *PRMT5-ISO1*) translated into full-length protein, another transcript *PRMT5* isoform e (NM_001282955.2, *PRMT5-ISO5*) is produced by the skipping of exon 3 and part of exon 4. The latter transcript can exhibit distinct localization and preferential control of critical genes for cell cycle arrest compared to the full-length PRMT5 [12]. In our previous results, *PRMT5-ISO5* has demonstrated its response to radiation in blood samples from irradiated HCC patients, suggesting the possibility of *PRMT5* splicing triggered by IR.

Herein, we identify that serine/arginine-rich splicing factor 3 (SRSF3) and heterogeneous nuclear ribonucleoprotein H 1 (HNRNPH1) have antagonistic interactions in regulating exon 3 and partial exon 4 skipping to generate *PRMT5-ISO5* induced by IR. The increase of *PRMT5-ISO5* contributes to the response of HCC cells to radiation and against xenograft tumor growth, which could be a potential therapeutic target in HCC progression.

Materials And Methods

Patients and bioinformatics analysis

The criteria for blood samples from HCC patients who received stereotactic body radiotherapy (SBRT) including 1) hepatocellular carcinoma with relatively preserved liver function (Child-Pugh classification A or B), 2) taking SBRT as the first treatment with biologically effective dose (BED) in correspondence from 80Gy to 100Gy, 3) without other comprehensive therapies affecting indicators in the blood such as

chemotherapeutic treatments. All the patients with the written informed consent and study protocols were approved by the Ethics Committee of Wenzhou medical university. RNA sequencing (RNA-seq) and analysis were completed by Novogene Biotech.

The patients' datasets derived from TSVdb TCGA Splicing Variants Database (http://www.tsvdb.com/plot.html) were analyzed using Kruskal-Wallis test and Kaplan-Meier Curves (Log-Rank Tests) in R software. Single-cell RNA sequencing (scRNA-seq) dataset (GSE149614) derived from the Gene Expression Omnibus database (https://www.ncbi.nlm.nih.gov/geo/) were preprocessed by using the Seurat package in R software. The harmony package and t-distributed stochastic neighbor embedding (t-SNE) algorithm were used to perform normalization, dimensionality reduction and cluster classification. Gene ontology (GO) analysis was conducted with clusterProfiler packages. GEPIA2[13] was used for expression correlation and survival analysis.

Cell culture

Three human HCC cell lines (Huh7, HepG2, and MHCC-97H cells) were cultured in Dulbecco's modified Eagle medium (DMEM) supplemented with 10% fetal bovine serum (FBS, Gibco, USA) and Penicillin/streptomycin at 37℃ with 5% CO2. Additional methods are provided in the Supporting Information.

IR treatment

X-Rad 320 Biological Irradiator (Precision X-Ray, USA) was used to irradiate HCC cells and xenograft at a dose rate of 300 cGy/min.

Plasmid construction and siRNAs

The *PRMT5*-minigene, a segment of the *PRMT5*, was amplified by polymerase chain reaction (PCR). The human HNRNPH1 and SRSF3 open reading frames (ORFs) were amplified by RT-PCR. The primers are listed in Supplementary Table S1. Next, the PCR products were gel-purified with the Gel Extraction Kit (Takara, China), and then in-fusion cloned into the pcDNA 3.1-*FLAG* vector which had been digested by BamHI and XhoI restriction endonucleases (NEB, China) using ExonArt Seamless Cloning and Assembly Kit (Exongen, China).

The normal siRNA and in vivo siRNA (2' O-methyl+5' cholesterol-modified) against *HNRNPH1* or *SRSF3*, and nonsense siRNA (RiboBio, China) were dissolved in RNase-free water for cell transfection, or phosphate buffered saline (5nmol siRNA with 50 μL PBS) for intratumoral injection. The sequences of si-*HNRNPH1* and si-*SRSF3* are shown in Supplementary Table S1.

Cell transfection

RNA interference and construct overexpression were carried out in 6-well plates using Lipofectamine 2000 (Invitrogen, USA) with 5μL siRNA (the final concentration of 50 nM), or 2.5 μg plasmid. For co-

transfection assay, 2 μg *PRMT5*-minigene plasmid was co-transfected with 4 μL siRNA (the final concentration of 40 nM) or 2μg plasmid in *PRMT5* KO cells cultivated in the 6-well plates. For investigation of HNRNPH1 and SRSF3 interaction, 4 μg *PRMT5*-minigene plasmid was co-transfected with total 4 μg plasmids mixture (pcDNA 3.1-*FLAG-HNRNPH1* plus pcDNA 3.1-*FLAG-SRSF3*) in *PRMT5* KO cells grew in the 60 mm petri dishes. The cells were harvested 48h post-transfection. The levels of *PRMT5-ISO5* were determined by RT-qPCR and the expression of HNRNPH1 and SRSF3 were detected by western-blot.

Generation of *PRMT5* KO clones

Cas9 lentivirus and *PRMT5*-sgRNA lentivirus were designed and generated (Cyagen Biosciences, China) in HEK 293T cell lines by co-transfection of psPAX2, pMD2.G, and Cas9 or *PRMT5*-sgRNA plasmids with a 4:3:1 ratio. A total of 2.5 μg plasmids were mixed with Lipofectamine 2000 reagent (Thermo Fisher Scientific, USA) in a well of 6-well plates when HEK 293T cells had 60-70% confluency. Huh7 and MHCC-97H cell lines were infected with Cas9 lentivirus for 24 h and then treated with hygromycin for 7-10 d. Subsequently, Cas9 positive cells were infected with *PRMT5*-sgRNA lentivirus for another 24 h and then treated with puromycin for 5-7 d. Furthermore, serial dilution was performed to generate single clones of stable *PRMT5* knockout (KO) cell lines. Finally, all the clones were determined *PRMT5* KO efficiency by western blot.

Cell proliferation

Cell proliferation was detected using cell counting Kit-8 kit (China). 1.5×10^3 Huh7 cells were seeded into 96 well plates and treated with IR. 0h, 24h, 48h and 72h post-IR treatment, 10μL CCK-8 solution was added to each well and incubated for 1.5h at 37℃. The absorbance at $A_{450\ nm}$ was measured on Spectra Max 190 plate reader (Molecular Devices, USA).

Reverse transcription-quantitative PCR and western blotting

Total RNA was extracted using RNAiso Plus (Takara, China) according to the manufacturer's protocol. Quantitative PCR analysis of *PRMT5-ISO5* was carried out with 10μL TB Green™ Premix Ex Taq™ II (Takara, China) by QuantStudio 3 Real-Time PCR System (Applied Biosystems, USA). The primers for RT-qPCR are shown in Supplementary Table S1.

Proteins extracted from cells and tissues were measured and heat-denatured. Equal amounts of proteins were separated using 10% or 12% SDS-PAGE and transferred on the PVDF membrane (Millipore, USA). After saturating, membranes were incubated with anti-PRMT5 (ab109451, Abcam, USA), anti- HNRNPH1 (ab10374, Abcam, USA), anti-SRSF3 (ab198291, Abcam, USA), anti-AKT1 (75692S, CST, USA), anti-GAPDH (60004-1-Ig, Proteintech, China), and subsequently incubated with HRP-conjugated secondary antibodies (Biosharp, China). Finally, membranes were detected using Pierce™ ECL Western Blotting Substrate (Thermo Scientific™, USA) and visualized with ChemiScope 6100 (CliNX Science Instruments, China).

RNA-immunoprecipitation

Cells were transfected with FLAG-tagged SRSF3 or HNRNPH1 using Lipofectamine 2000 reagent (Thermo Fisher Scientific, USA). 48 h post-transfection, cells were washed and collected in lysis buffer (10 mM Tris-HCl (pH 7.5), 100mM NaCl, 5mM $MgCl_2$0.5% NP-40, 1% Triton X-100) containing EDTA-free Protease Inhibitor Cocktail (Roche, Switzerland), 1mM DTT (Thermo Scientific™, USA) and 200 units/mL RNase OUT (Invitrogen, USA). Then 10% of cell lysate was taken as “input” and the remains were divided into equal amounts and incubated overnight at 4℃ with anti-FLAG magnetic beads (Bimake, China) or pre-prepared IgG-protein A/G magnetic beads (Bimake, China). Subsequently, all the mixtures were washed 6 times with 1×NT-2 buffer (50 mM Tris-HCl (pH 7.5), 150 mM NaCl, 1 mM $MgCl_2$, 0.05% NP-40) using DynaMag^{TM}-2 Magnet (Invitrogen, USA). Next, washed samples were digested at 55℃ for 30 min with Proteinase K digestion buffer (1×NT-2 buffer containing 1 % SDS, 1.2mg/mL Proteinase K). Finally, the immunoprecipitated RNA was extracted using RNAiso Plus (Takara, China). Fold enrichment of target region was determined after normalization to the input and compared with IgG control. The primers for RT-qPCR are shown in Supplementary Table S1.

Hydrodynamic tail-vein injection and *Prmt5* conditional knockout experiments

Male *Prmt5*$^{flox/flox}$-Alb-CreERT2 mice with C57BL/6J background (4-5 weeks old) were generated and purchased from Cyagen Biosciences. The mice were housed under pathogen-free conditions with a 12 h light/dark cycle and freely accessed to water and food. pCMV(CAT)T7-SB100 and pT3-myr-AKT-HA were bought from Fenghui Biotechnology (Addgene plasmids #34879 and #31789), and pT3-EF1α-NRasV12 (RPT-ZL 2101C2) was purchased from RiboBio. After acclimation for a week, hydrodynamic tail-vein injection (HTVi) of a volume equivalent to 10% body weight of endotoxin-free plasmids (10 μg of pCMV(CAT)T7-SB100, 10 μg of pT3-myr-AKT-HA, and 10 μg of pT3-EF1α-NRasV12 for each mice [14-16]) dissolved in PBS was given to *Prmt5*$^{flox/flox}$-Alb-CreERT2 mice within 7s [17-18]. Registering morbidity (white spots presented on the liver) according to pre-specified criteria, the mice were randomly divided into conditional KO (CKO) cohort and non-CKO control around 7.4 weeks post-HTVi. The mice from the CKO group were received continuous intraperitoneal injection of 100 μL tamoxifen (pre-dissolved in corn oil at 10 mg/mL, 40 mg/kg per mice, Sigma-Aldrich, USA) for 7 days. The mice were euthanized, and liver (tumor) tissues were collected for further analyses. All animal care and experimental procedures were carried out in accordance with protocols approved by Wenzhou Medical University Institutional Animal Care and Use Committee.

Xenograft model and treatments

Male BALB/C nude mice (4-5 weeks old, Zhejiang Vital River Laboratory Animal Technology) were kept under pathogen-free conditions with a 12 h light/dark cycle and freely accessed to water and food. After acclimation for a week, 1×10^7 Huh7 cells were mixed with Matrigel Basement Membrane Matrix (BD, USA) at 4℃ and then injected into the right flank of nude mice. When the tumors were visible (160 mm^3 in volume), the mice were divided into 4 groups and respectively treated with 1) 15Gy IR, 2) 15Gy IR, and

intratumoral injection of si-*HNRNPH1* (5 nmol for each), 3) 15Gy IR, and intratumoral injection of si-*SRSF3* (5 nmol for each)[19], and 4) untreated control. All animal care and experimental procedures were carried out in accordance with protocols approved by Wenzhou Medical University Institutional Animal Care and Use Committee.

Tumor growth and histochemistry assay

The xenograft tumor volume was measured every 2 days and calculated as follows: volume = longest tumor diameter × (shortest tumor diameter)^2/2. At the end of the experiment, mice were sacrificed by euthanasia, tumor tissues were excised, weighted, images captured, and immunohistochemistry analyzed.

Liver (tumor) tissue sections were paraffin-embedded, deparaffinized, and rehydrated, followed by hematoxylin and eosin (H&E) staining. For detection of lipid droplets, liver tissue sections were incubated with oil red O dye and washed with 60% isopropanol. The images were captured and have been evaluated by an experienced pathologist (SFH).

Statistical analysis

Statistical analysis for biological assays was performed by Graphpad Prism 7 software, using one way or two-way ANOVA, and two-tailed unpaired t-test, as appropriate. All data are presented as mean ± S.D. differences were considered statistically significant if $P<0.05$, $^{*}P<0.05$, $^{**}P<0.01$, $^{***}P<0.001$, $^{****}P<0.0001$.

Results

The increase of PRMT5-ISO5 improves the poor prognosis of HCC

The splice variant *PRMT5-ISO5* lacks exon 3 and part of exon 4 (Fig. 1a), which encodes a shorter isoform and translates the short protein. Using GEPIA2 web server [13], we found that the level of *PRMT5* was significantly higher in tumors than normal tissues in liver hepatocellular carcinoma (LIHC), lung adenocarcinoma (LUAD) and lung squamous cell carcinoma (LUSC) among 23 types of cancers (Supplementary Fig. 1a). Interestingly, the level of *PRMT5-ISO1* (named PRMT-003 in GEPIA2) presented similar distribution among these three cancer types, while the level of *PRMT5-ISO5* (named PRMT5-010 in GEPIA2) showed different distribution (the shape of violin-plots) in LIHC compared to the others (Supplementary Fig. 1b). Further investigation revealed that HCC patients with higher level of *PRMT5-ISO1* survived for significantly shorter times than lower level patients, while high level of *PRMT5-ISO5* improved the poor prognosis of HCC patients, though both transcripts showed increased expression in tumor (Fig. 1b, c). Subsequently, we also observed that the decrease of *PRMT5-ISO1* and the increase of *PRMT5-ISO5* in blood samples from HCC patients receiving SBRT (Supplementary Fig. 1c). These results indicated that the increase of *PRMT5-ISO5* might play a positive role in radiotherapy of HCC patients.

To further confirm that IR could raise the level of *PRMT5-ISO5* transcript, three HCC cell lines (Huh7, HepG2, and MHCC-97H cells) were treated with IR (10Gy, 15Gy, and 20Gy) as shown in Supplementary Fig. 1d. By performing the RT-qPCR assay, we found that *PRMT5-ISO5* steadily and continuously increased in Huh7 cells after IR (Fig. 1d). Unexpectedly, *PRMT5-ISO5* rapidly descended in MHCC-97H cells while mild decreased then recovered in HepG2 cells (Fig. 1e and Supplementary Fig. 1e), showing that the changes of *PRMT5-ISO5* level were different among HCC cells. Besides, IR also inhibited the cell proliferation of Huh7 cells (Fig. 1f), supporting that the increase of *PRMT5-ISO5* induced by IR might improve the poor prognosis of HCC patients, at least in part, depending on cell proliferation-inhibition in Huh7 cells.

Figure 1 is about here

IR induces PRMT5-ISO5 **transcript by virtue of SRSF3 and HNRNPH1**

Subsequently, we analyzed RNA-seq data and found the vast majority of genes downregulated after IR (Fig. 2a, b). With further exploration, genes with significant change were observed to enrich in RNA splicing pathway, including dozens of representative splicing factors (Fig. 2c). To verify the potential splicing regulators induced by IR, differential expression, overall survival and correlation analysis were performed among these splicing factors with significant change. Considering these signatures above, though we found IR induced remarkably decrease of SRSF2, SRSF3, SRSF5, SRSF6 and SRSF11, only SRSF3 and SRSF11 showed significance in differential expression between LIHC patients and normal controls, as well as the association with poor prognosis of LIHC patients (Fig. 2d, f, and Supplementary Fig. S2a-c). Further consideration indicated that SRSF3 showed higher correlation means stronger relationship with PRMT5 than SRSF11 (Fig. 2g and Supplementary Fig. S2d). Besides, by analyzing the HCC scRNA-seq dataset (GSE149614), more than 70,000 single-cell transcriptomes for 10 HCC patients were obtained. After standardization and dimensionality reduction and clustering, 15 clusters of cells were defined using the clusterProfiler package based on the transcriptional levels of SRSF3 and HNRNPH1 (Fig. 2h and Supplementary Fig. S2e, f). Specifically, genes with significant change from 2 cell populations (PCT1 and PCT2) which were identified with high level of SRSF3 were observed to enrich in RNA splicing pathway (Fig. 2i, j). These results suggested that SRSF3 might be in a dominant position in regulating *PRMT5* splicing.

With the assumption that SRSF3 and HNRNPH1[5] might be the effectors in *PRMT5* splicing induced by IR, we observed SRSF3 continuously decreased in Huh7 cells while decreased then recovered in MHCC-97H cells and HepG2 cells after IR treatment (Fig. 2k and Supplementary Fig. S2g). Although HNRNPH1 quickly decreased then recovered, the increase of *PRMT5-ISO5* occurred within 24 h (Supplementary Fig. S2h), suggesting that the level changes of SRSF3 and HNRNPH1 might have their effects in the early stage. Expectedly, SRSF3 sharply decreased in Huh7 cells within 1h while stably expressed in MHCC-97H cells until 12h, while HNRNPH1 changes were similar between the two HCC cells (Fig. 2l). It suggests that SRSF3 and HNRNPH1 might be the endogenous regulators of *PRMT5-ISO5* induced by IR, and SRSF3 probably played a primary role in this process.

Figure 2 is about here

SRSF3 and HNRNPH1 have the opposite effects on PRMT5 AS

To evaluate the effect of SRSF3 and HNRNPH1 on *PRMT5-ISO5* transcript, wide type Huh7 and MHCC-97H cells were transfected with si-*HNRNPH1* or si-*SRSF3* (Fig. 3a and Supplementary Fig. S3a, b). We observed that HNRNPH1 depletion caused a reduction of *PRMT5-ISO5*, while SRSF3 silencing led to the increase of *PRMT5-ISO5*, both in Huh7 and MHCC-97H cells (Fig. 3b). Furthermore, we also found that SRSF3 overexpression inhibited the increase of *PRMT5-ISO5* induced by IR in Huh7 cells (Fig. 3c).Though HNRNPH1 silencing slightly weakened the level of *PRMT5-ISO5* induced by IR, there was no significance compared with control. In MHCC-97H cells, HNRNPH1 depletion diminished *PRMT5-ISO5* levels compared with control (siNC) in most of the time, but SRSF3 silencing could not recover the downregulation of *PRMT5-ISO5* induced by IR (Fig. 3d). It seems that IR somehow leads to a more efficient change of *PRMT5-ISO5* levels compared with the interference of SRSF3 and HNRNPH1 in HCC cells. Curiously, SRSF3 expression seemed to be more affected with IR treatment in Huh7 cells, while HNRNPH1 interfere was more influential in rescuing *PRMT5-ISO5* downregulation in MHCC-97H cells treated by IR.

Regarding other effective factors, such as *PRMT5-AS1* (an antisense transcript of *PRMT5*) [20], we generated multiple single *PRMT5* KO clones in Huh7 and MHCC-97H cell lines using the CRISPR/Cas9 system and serial dilution method (Supplementary Fig. 3c). Despite screening for ~ 100 single clones of each cell line, though we seldom observed complete depletion of *PRMT5* at the protein level, the transcriptional levels of *PRMT5*-minigene achieved dozens times of residual expression of endogenous *PRMT5* mRNA (Supplementary Fig. 3d). Subsequently, co-transfection of *PRMT5*-minigene construct and si-*HNRNPH1* or si-*SRSF3* were performed in *PRMT5* KO cells to simulate AS of *PRMT5* (Fig. 4c). We found that IR still resulted in the increase of *PRMT5-ISO5* in $PRMT5^{minigene}$ Huh7 cells. Besides, IR still promoted PRMT5 splicing and SRSF3 silencing showed the impact on *PRMT5* splicing somehow, compared with wild type Huh7 cells (Fig. 3c, e). Meanwhile, IR-induced the decrease of *PRMT5-ISO5* was constrained in $PRMT5^{minigene}$ MHCC-97H cells, though the silencing of splicing factors still had appropriate effects on *PRMT5* splicing (Fig. 3d, f). The results above indicated that there might be other interferences like *PRMT5-AS1* depended on 3'-terminal sequences of *PRMT5* precursor mRNA (pre-mRNA) to contribute to the change of *PRMT5-ISO5* induced by IR, which was worth exploring further.

Figure 3 is about here

The antagonistic interaction of SRSF3 and HNRNPH1 dependents on their competitive binding with PRMT5

To verify the interaction of SRSF3 and HNRNPH1 on *PRMT5* AS, co-transfection of *PRMT5*-minigene and regulators (a mixture of SRSF3 construct and HNRNPH1 construct) was performed in *PRMT5* KO cells. We observed that, along with gradient decrease of exogenous HNRNPH1, gradient increase of exogenous SRSF3 could inhibit *PRMT5-ISO5* by degrees (Fig. 4a-d). In addition, the increase of *PRMT5-ISO5* seemed

to be more sensitive to SRSF3 upregulation in *PRMT5*^{minigene} Huh7 cells, while the effect of HNRNPH1 was prominent in *PRMT5*^{minigene} MHCC-97H cells.

Considering the potential binding sites of SRSF3 and HNRNPH1 on the position from exon 2 to exon 4 of *PRMT5* gene in the Splice Aid database (http://193.206.120.249/splicing_tissue.html), we designed 4 pairs of primers targeted to the potential binding sites (Fig. 4e, f). By performing RIP-qPCR assay, we found that both SRSF3 and HNRNPH1 were significantly enriched on the region around 3' splicing site of intron 2 and alternative 3' splicing site on exon 4 of *PRMT5* (Fig. 4g, h). In addition, the fold enrichment of SRSF3 was higher than HNRNPH1 in Huh7 cells (Fig. 4g), while HNRNPH1 was prior to enrich on *PRMT5* in MHCC-97H cells (Fig. 4h). For endogenous SRSF3 and HNRNPH1, though we didn't observe significant differences on the fold enrichment of HNRNPH1 using anti-HNRNPH1 antibody in cells treated with si-*SRSF3* (37.5 and 50 μM), the faint amount of *PRMT5* pre-mRNA acquired by anti-*HNRNPH1* antibody limited our investigation (data didn't show).

Figure 4 is about here

IR-induced PRMT5-ISO5 **inhibits tumor growth in vivo**

To evaluate the tumorigenic effect of IR accompanied with RNA interference which were associated with *PRMT5-ISO5* transcript, a xenograft HCC model was constructed via subcutaneous injection of Huh7 cells (Fig. 5a). After 8 days post-treatment, we confirmed the significant downregulation of SRSF3 in all experimental groups (Fig. 5b and Supplementary Fig. 4a). We found that, although HNRNPH1 silencing reversed the increase of *PRMT5-ISO5* induced by IR while SRSF3 knockdown reinforced it, there was no remarkable difference in tumor growth among experimental groups (Fig. 5c). Furthermore, compared with the control group, tumor sizes and tumor growth were significantly reduced in experimental groups (Fig. 5d). Besides, accompanied by lymphocytic infiltration, varying degrees of cell degeneration and necrosis were observed in tumor tissues as well (Fig. 5e). These results suggested that IR inhibited HCC tumor growth and caused tumor regression partially due to the increase of *PRMT5-ISO5* transcript.

Figure 5 is about here

So far, some researches proved the high level of PRMT5 was closely associated with HCC, the limitation is the usage of HCC cell lines or xenograft models by passing over the efficacy in the remedy of spontaneous HCC [21]. To confirm whether liver-specific Prmt5 deficiency could achieve remission of autochthonous HCC, Akt/N-Ras-based HTVi and tamoxifen-inducible deletion of Prmt5 specifically within liver were used in *Prmt5*$^{flox/flox}$-Alb-CreERT2 mouse models (Fig. 6a). Previously, intraperitoneal injection of tamoxifen were performed to acquire liver-specific Prmt5 KO. We confirmed significant KO efficiency of Prmt5 in liver tissues within continuous injection for 5 and 7 days, and negative or trace amount of Prmt5 was detected 30 days after completing the injection (Supplementary Fig. 4b). Furthermore, regularly sacrificing one cohort of C57BL/6J mice after HTVi, we found that exogenetic Akt1 expression, the number of tumor nodules and the size of liver were increased within HCC progression, along with splenomegaly (Supplementary Fig. 4c, d). Besides, H&E and Oil Red O staining of liver sections

demonstrated that vacuolar denaturation, inflammation and intracellular lipid accumulation presented on the liver after HTVi treatment (Supplementary Fig. 4e). In this study, when tumors were visible at day 52 post-HTVi treatment, intraperitoneal injection of tamoxifen was performed in *Prmt5*$^{flox/flox}$-Alb-CreERT2 mice. At day 62 post-HTVi treatment, all the mice were sacrificed. In the results, we observed the exogenous expression of Akt1 remarkably reduced, along with Prmt5 deficiency (Fig. 6b). In addition, dramatically decreased in number of tumor nodules was visible in the surface of liver from liver-specific Prmt5 KO mice (Fig. 6c). H&E and Oil Red O staining of liver sections from liver-specific Prmt5 KO mice also showed reduced pathology associated with steatosis, hepatocyte bubble morohology, and inflammation in livers (Fig. 6d), suggesting that Prmt5 deficiency prominently inhibits Akt/N-Ras-derived hepatocarcinogenesis.

Figure 6 is about here

Discussion

According to the 2020 WHO report (Globocan 2020), HCC, with the fourth rank of new cases and the second rank of deaths among multiple cancers in China, has remained to show the increased mortality and poor 5-year prevalence. Considering that more than 70% of patients harboring high tumor burden or liver dysfunction are still unsuitable for definitive resection [22]. SBRT was a new non-invasive treatment for HCC patients who are not suitable for radical surgery [23]. Yet, there is still insufficient evidence on the molecular mechanism of SBRT in HCC patients.

Transcriptomic analyses have revealed that splicing aberrations, not just expression dysregulation of certain genes occur in HCC tumor tissues, which are correlated with HCC patient survival [24]. Herein, we reported *PRMT5-ISO5*, a specific splicing variant of *PRMT5*, increased in blood samples from HCC patients who received SBRT. *PRMT5-ISO5* lacks exon 3 and partial exon 4 and translates the shorter protein, which regulates genes involved in apoptosis and differentiation [25]. By observing the high level of *PRMT5-ISO5* is associated with improvement of poor prognosis of HCC patients, we inferred that *PRMT5* splicing responded to radiation probably contributed to the effect of radiotherapy for HCC.

Current evidence has indicated that aberrant expression of splicing regulators often elicits changes in AS and promotes HCC development, and SR/hnRNP proteins significantly affect responses to chemotherapy[25–29]. HNRNPH1, as a member of the hnRNPs family, is reported to contribute to splicing involved in tumorigenic progress of Burkitt lymphoma and HCC[30–32]. Specifically, HNRNPH/F can inhibit the combination of U2AF65 and the polypyrimidine tract by its binding to G tracts which is situated upstream from exon 3 of *PRMT5* [12]. On the other hand, as an unfavorable prognostic predictor in HCC [30, 33], the decreased expression of SRSF3 can induce p53β transcript and lead to p53-mediated cellular senescence [34]. Regarding that SRSF3 and HNRNPH1 have effects on regulating the production of HER2 splice variants in invasive breast cancer [35], we found a potential interaction of SRSF3 and HNRNPH1 in regulating *PRMT5-ISO5* in response to radiation treatment. Unexpectedly, we observed that *PRMT5-ISO5*

increased in Huh7 cells but decreased in MHCC-97H cells induced by IR, suggesting that SRSF3 might be more responsive to IR and more efficient in regulating *PRMT5* splicing in Huh7 cells. Furthermore, we identified that HNRNPH1 silencing led to *PRMT5-ISO5* decrease while SRSF3 silencing resulted in the increase of *PRMT5-ISO5*. Although HNRNPH1 depletion showed its limited inhibition on *PRMT5-ISO5* in *PRMT5*^{mini} Huh7 cells, compared with wildtype Huh7 cells. This might be partly due to the loss of PRMT5 which was reported to be the methylase of HNRNPH1 [36]. Besides, IR appeared to be less effective in reducing *PRMT5-ISO5* in *PRMT5*^{mini} MHCC-97H cells, suggesting that the absence of *PRMT5* 3'-terminal might eliminate the effect of *PRMT5-AS1* on IR-induced *PRMT5*-minigene AS [20]. By observing that SRSF3 and HNRNPH1 shared similar affinities to the binding region around 3' splicing site of intron 2 and alternative 3' splicing site on exon 4, we indicated that SRSF3 and HNRNPH1 probably have a competitive interaction on binding to *PRMT5* pre-mRNA. However, there were minor differences between Huh7 and MHCC-97H cells on the fold enrichment of SRSF3 and HNRNPH1 binding to the intron 3 and partial Exon 4, which might contribute to varying *PRMT5-ISO5* between the two HCC cells. Still, the molecular mechanism of IR-induced *PRMT5-ISO5* transcriptional changes between Huh7 and MHCC-97H cells is needed to study in-depth.

In vivo, we revealed that tumor volume reduction and structural damage presented in xenograft tumors after IR treatment. Although intratumoral injection of in vivo siRNA either enhanced or slightly interfered with the anti-tumorigenic effect of IR, *PRMT5-ISO5* probably improved the efficiency of radiotherapy.

Accumulating researches indicate that PRMT5 might be a potential therapeutic target in HCC, the disadvantage of experimentally induced spontaneous HCC models limits studies in vivo. Currently, a transposon-based liver-specific delivery through HTVi becomes the perfect technique for the establishment of HCC to study the potential oncogenic genes [15, 37–38]. Akt/N-Ras-based HTVi technology is reported to rapidly induce HCC formation accompanied by fatty change lesions [15]. By recapitulating aberrant lipid metabolism involved in the HCC development, we observed that liver specific *Prmt5* KO decelerated tumorigenesis of Akt/N-Ras-transformed hepatocytes, compared to non-CKO group. Besides, recent studies also showed that the inhibition of PRMT5 with immune checkpoint therapy diminished growth of murine melanoma tumors and enhanced therapeutic efficacy [39], and amounts of suppressive macrophages infiltrate and exhausted-like phenotypes tumor-associated antigen-specific CD8 + T cells presented during Akt/N-Ras-derived HCC progression [15, 37, 40]. It suggests that PRMT5 depletion inhibits Akt/N-Ras-derived hepatocarcinogenesis might partly due to the dysfunction of methylating Akt1 for oncogenic activation and improve immune dysregulation. Considering that murine *Prmt5* has different splicing isoforms compared to human *PRMT5-ISO5*, whether *PRMT5-ISO5* contributes to the anti-tumorigenic function which is analogous to Prmt5 depletion in primary HCC is worth investigating further. And our study provides a suitable model to further elucidate the function of *PRMT5-ISO5* on HCC progression and treatment in vivo.

In summary, we presented a potential mechanism that SRSF3 and HNRNPH1 play antagonistic roles in regulating *PRMT5-ISO5* induced by IR, owing to their competitive binding with *PRMT5* pre-mRNA (Fig. 7).

The increase of *PRMT5-ISO5* improves the radiosensitivity of HCC in response to radiation treatment, and Akt/N-Ras-derived spontaneoous HCC with liver-specific *Prmt5* KO model provides a rationale to investigate the role of the specific spliced isoform on HCC therapy.

Figure 7 is about here

Abbreviations

PRMT5, arginine methyltransferase 5, *PRMT5-ISO5*, *PRMT5* isoform e, HNRNPH1, heterogeneous nuclear ribonucleoprotein H 1, SRSF3, serine/arginine-rich splicing factor 3, pre-mRNA, precursor mRNA, SBRT, stereotactic body radiotherapy, IR, ionizing radiation, 5'ss, 5' splicing site, 3'ss, 3' splicing site, RBPs, RNA-binding proteins, AS, alternative splicing, exon 3-4A, exon 3 and partial exon 4, RIP: RNA immunoprecipitation, HTVi, hydrodynamic tail-vein injection, AKT: protein kinase B, N-RAS: neuroblastoma RAS viral oncogene homolog, H&E: hematoxylin and eosin.

Declarations

Authors' contributions

C Wen and X Liu designed research and wrote the manuscript, C Wen, L Li, Z Liang, Y Ying and P Li performed the in vitro experiments and generated data, C Wen, S Qu, H Chen and J Dai analyzed the data, C Wen, Z Tian, T Chen, M Li and Y Liu performed in vivo experiments and analyzed the data, S Ma and X Liu provided critical evaluation of experimental data and edited the manuscript. All authors reviewed and approved the manuscript.

Funding

This work was supported by National Natural Science Foundation of China (81972969 and 81773363), and Zhejiang Provincial Medical and Health Science and Technology Project of China (2018KY508). The funding body had no role in the design of the study, collection, analysis, and interpretation of the data, or preparation of the manuscript.

Acknowledgements

We thank to Prof. Haishan Huang and Prof. Hezhi Fang in School of Laboratory Medicine and Life Science, Wenzhou Medical University for help during the advice and process of histochemistry assay and RNA immunoprecipitation.

Availability of data and materials

The RNA-seq datasets supporting the conclusions of this article are included within the article and its supplementary files. The scRNA-seq datasets presented in this study can be found below: https://www.ncbi.nlm.nih.gov/geo/query/acc.cgi?acc=GSE149614.

Ethics approval and consent to participate

The present study was approved by the Ethics Committee of Wenzhou medical university and Institutional Animal Care and Use Committee of Wenzhou Medical University.

Consent for publication

We have received consents from individual patients who have participated in this study. The consent forms will be provided upon request.

Competing interests

The authors declare no potential conflicts of interest.

References

1. Kim H, Ronai ZA. PRMT5 function and targeting in cancer. Cell Stress. 2020 Jul 13,4(8):199-215. doi: 10.15698/cst2020.08.228.
2. Gullà A, Hideshima T, Bianchi G, Fulciniti M, Kemal Samur M, Qi J, et al. Protein arginine methyltransferase 5 has prognostic relevance and is a druggable target in multiple myeloma. Leukemia. 2018 Apr,32(4):996-1002. doi: 10.1038/leu.2017.334.
3. Jarrold J, Davies CC. PRMTs and Arginine Methylation: Cancer's Best-Kept Secret? Trends Mol Med. 2019 Nov,25(11):993-1009. doi: 10.1016/j.molmed.2019.05.007.
4. Tan L, Xiao K, Ye Y, Liang H, Chen M, Luo J, et al. High PRMT5 expression is associated with poor overall survival and tumor progression in bladder cancer. Aging (Albany NY). 2020 May 11,12(9):8728-8741. doi: 10.18632/aging.103198.
5. Liang Z, Wen C, Jiang H, Ma S, Liu X. Protein Arginine Methyltransferase 5 Functions via Interacting Proteins. Front Cell Dev Biol. 2021 Aug 27,9:725301. doi: 10.3389/fcell.2021.725301.
6. Wei X, Yang J, Adair SJ, Ozturk H, Kuscu C, Lee KY, et al. Targeted CRISPR screening identifies PRMT5 as synthetic lethality combinatorial target with gemcitabine in pancreatic cancer cells. Proc Natl Acad Sci U S A. 2020 Nov 10,117(45):28068-28079. doi: 10.1073/pnas.2009899117.
7. Luo Y, Gao Y, Liu W, Yang Y, Jiang J, Wang Y, et al. Myelocytomatosis-Protein Arginine N-Methyltransferase 5 Axis Defines the Tumorigenesis and Immune Response in Hepatocellular Carcinoma. Hepatology. 2021 Oct,74(4):1932-1951. doi: 10.1002/hep.31864.
8. Farina AR, Cappabianca L, Sebastiano M, Zelli V, Guadagni S, Mackay AR. Hypoxia-induced alternative splicing: the 11th Hallmark of Cancer. J Exp Clin Cancer Res. 2020 Jun 15,39(1):110. doi: 10.1186/s13046-020-01616-9.
9. Ule J, Blencowe BJ. Alternative Splicing Regulatory Networks: Functions, Mechanisms, and Evolution. Mol Cell. 2019 Oct 17,76(2):329-345. doi: 10.1016/j.molcel.2019.09.017.

10. Lv Y, Zhang W, Zhao J, Sun B, Qi Y, Ji H, et al. SRSF1 inhibits autophagy through regulating Bcl-x splicing and interacting with PIK3C3 in lung cancer. Signal Transduct Target Ther. 2021 Mar 5,6(1):108. doi: 10.1038/s41392-021-00495-6.
11. Kędzierska H, Piekiełko-Witkowska A. Splicing factors of SR and hnRNP families as regulators of apoptosis in cancer. Cancer Lett. 2017 Jun 28,396:53-65. doi: 10.1016/j.canlet.2017.03.013.
12. Sohail M, Xie J. Evolutionary emergence of a novel splice variant with an opposite effect on the cell cycle. Mol Cell Biol. 2015 Jun,35(12):2203-14. doi: 10.1128/MCB.00190-15.
13. Tang Z, Kang B, Li C, Chen T, Zhang Z. GEPIA2: an enhanced web server for large-scale expression profiling and interactive analysis. Nucleic Acids Res. 2019 Jul 2,47(W1):W556-W560. doi: 10.1093/nar/gkz430.
14. Mátés L, Chuah MK, Belay E, Jerchow B, Manoj N, Acosta-Sanchez A, et al. Molecular evolution of a novel hyperactive Sleeping Beauty transposase enables robust stable gene transfer in vertebrates. Nat Genet. 2009 Jun,41(6):753-61. doi: 10.1038/ng.343.
15. Liu YT, Tseng TC, Soong RS, Peng CY, Cheng YH, Huang SF, et al. A novel spontaneous hepatocellular carcinoma mouse model for studying T-cell exhaustion in the tumor microenvironment. J Immunother Cancer. 2018 Dec 7,6(1):144. doi: 10.1186/s40425-018-0462-3.
16. Wiesner SM, Decker SA, Larson JD, Ericson K, Forster C, Gallardo JL, et al. De novo induction of genetically engineered brain tumors in mice using plasmid DNA. Cancer Res. 2009 Jan 15,69(2):431-9. doi: 10.1158/0008-5472.CAN-08-1800.
17. Kang TW, Yevsa T, Woller N, Hoenicke L, Wuestefeld T, Dauch D, et al. Senescence surveillance of pre-malignant hepatocytes limits liver cancer development. Nature. 2011 Nov 9,479(7374):547-51. doi: 10.1038/nature10599.
18. Rudalska R, Dauch D, Longerich T, McJunkin K, Wuestefeld T, Kang TW, et al. In vivo RNAi screening identifies a mechanism of sorafenib resistance in liver cancer. Nat Med. 2014 Oct,20(10):1138-46. doi: 10.1038/nm.3679.
19. Banerjee D, Gakhar G, Madgwick D, Hurt A, Takemoto D, Nguyen TA. A novel role of gap junction connexin46 protein to protect breast tumors from hypoxia. Int J Cancer. 2010 Aug 15,127(4):839-48. doi: 10.1002/ijc.25107.
20. Baytak E, Gong Q, Akman B, Yuan H, Chan WC, Küçük C. Whole transcriptome analysis reveals dysregulated oncogenic lncRNAs in natural killer/T-cell lymphoma and establishes MIR155HG as a target of PRDM1. Tumour Biol. 2017 May,39(5):1010428317701648. doi: 10.1177/1010428317701648.
21. Luo Y, Gao Y, Liu W, Yang Y, Jiang J, Wang Y, et al. Myelocytomatosis-Protein Arginine N-Methyltransferase 5 Axis Defines the Tumorigenesis and Immune Response in Hepatocellular Carcinoma. Hepatology. 2021 Oct,74(4):1932-1951. doi: 10.1002/hep.31864.
22. Liu X, Qin S. Immune Checkpoint Inhibitors in Hepatocellular Carcinoma: Opportunities and Challenges. Oncologist. 2019 Feb,24(Suppl 1):S3-S10. doi: 10.1634/theoncologist.2019-IO-S1-s01.

23. Zhang T, Sun J, He W, Li H, Piao J, Xu H, et al. Stereotactic body radiation therapy as an effective and safe treatment for small hepatocellular carcinoma. BMC Cancer. 2018 Apr 20,18(1):451. doi: 10.1186/s12885-018-4359-9.
24. Sohail M, Zhang M, Litchfield D, Wang L, Kung S, Xie J. Differential expression, distinct localization and opposite effect on Golgi structure and cell differentiation by a novel splice variant of human PRMT5. Biochim Biophys Acta. 2015 Oct,1853(10 Pt A):2444-52. doi: 10.1016/j.bbamcr.2015.07.003.
25. Li S, Hu Z, Zhao Y, Huang S, He X. Transcriptome-Wide Analysis Reveals the Landscape of Aberrant Alternative Splicing Events in Liver Cancer. Hepatology. 2019 Jan,69(1):359-375. doi: 10.1002/hep.30158.
26. Li T, Li S, Chen D, Chen B, Yu T, Zhao F, et al. Transcriptomic analyses of RNA-binding proteins reveal eIF3c promotes cell proliferation in hepatocellular carcinoma. Cancer Sci. 2017 May,108(5):877-885. doi: 10.1111/cas.13209.
27. Chen H, Gao F, He M, Ding XF, Wong AM, Sze SC, et al. Long-Read RNA Sequencing Identifies Alternative Splice Variants in Hepatocellular Carcinoma and Tumor-Specific Isoforms. Hepatology. 2019 Sep,70(3):1011-1025. doi: 10.1002/hep.30500.
28. Zhou HZ, Li F, Cheng ST, Xu Y, Deng HJ, Gu DY, et al. DDX17-regulated alternative splicing that produced an oncogenic isoform of PXN-AS1 to promote HCC metastasis. Hepatology. 2022 Apr,75(4):847-865. doi: 10.1002/hep.32195.
29. Kędzierska H, Piekiełko-Witkowska A. Splicing factors of SR and hnRNP families as regulators of apoptosis in cancer. Cancer Lett. 2017 Jun 28,396:53-65. doi: 10.1016/j.canlet.2017.03.013.
30. Yamazaki T, Liu L, Conlon EG, Manley JL. Burkitt lymphoma-related TCF3 mutations alter TCF3 alternative splicing by disrupting hnRNPH1 binding. RNA Biol. 2020 Oct,17(10):1383-1390. doi: 10.1080/15476286.2020.1772559.
31. Chettouh H, Fartoux L, Aoudjehane L, Wendum D, Clapéron A, Chrétien Y, et al. Mitogenic insulin receptor-A is overexpressed in human hepatocellular carcinoma due to EGFR-mediated dysregulation of RNA splicing factors. Cancer Res. 2013 Jul 1,73(13):3974-86. doi: 10.1158/0008-5472.CAN-12-3824.
32. Li X, Qian X, Peng LX, Jiang Y, Hawke DH, Zheng Y, et al. A splicing switch from ketohexokinase-C to ketohexokinase-A drives hepatocellular carcinoma formation. Nat Cell Biol. 2016 May,18(5):561-71. doi: 10.1038/ncb3338.
33. Corbo C, Orrù S, Salvatore F. SRp20: an overview of its role in human diseases. Biochem Biophys Res Commun. 2013 Jun 21,436(1):1-5. doi: 10.1016/j.bbrc.2013.05.027.
34. Tang Y, Horikawa I, Ajiro M, Robles AI, Fujita K, Mondal AM, et al. Downregulation of splicing factor SRSF3 induces p53β, an alternatively spliced isoform of p53 that promotes cellular senescence. Oncogene. 2013 May 30,32(22):2792-8. doi: 10.1038/onc.2012.288.
35. Gautrey H, Jackson C, Dittrich AL, Browell D, Lennard T, Tyson-Capper A. SRSF3 and hnRNP H1 regulate a splicing hotspot of HER2 in breast cancer cells. RNA Biol. 2015,12(10):1139-51. doi:

10.1080/15476286.2015.1076610.

36. Musiani D, Bok J, Massignani E, Wu L, Tabaglio T, Ippolito MR, et al. Proteomics profiling of arginine methylation defines PRMT5 substrate specificity. Sci Signal. 2019 Apr 2,12(575):eaat8388. doi: 10.1126/scisignal.aat8388.
37. Wu M, Xia X, Hu J, Fowlkes NW, Li S. WSX1 act as a tumor suppressor in hepatocellular carcinoma by downregulating neoplastic PD-L1 expression. Nat Commun. 2021 Jun 9,12(1):3500. doi: 10.1038/s41467-021-23864-9.
38. Qiao Y, Wang J, Karagoz E, Liang B, Song X, Shang R, et al. Axis inhibition protein 1 (Axin1) Deletion-Induced Hepatocarcinogenesis Requires Intact β-Catenin but Not Notch Cascade in Mice. Hepatology. 2019 Dec,70(6):2003-2017. doi: 10.1002/hep.30556.
39. Kim H, Kim H, Feng Y, Li Y, Tamiya H, Tocci S, et al. PRMT5 control of cGAS/STING and NLRC5 pathways defines melanoma response to antitumor immunity. Sci Transl Med. 2020 Jul 8,12(551):eaaz5683. doi: 10.1126/scitranslmed.aaz5683.
40. Thorsson V, Gibbs DL, Brown SD, Wolf D, Bortone DS, Ou Yang TH, et al. The Immune Landscape of Cancer. Immunity. 2018 Apr 17,48(4):812-830.e14. doi: 10.1016/j.immuni.2018.03.023.

Figures

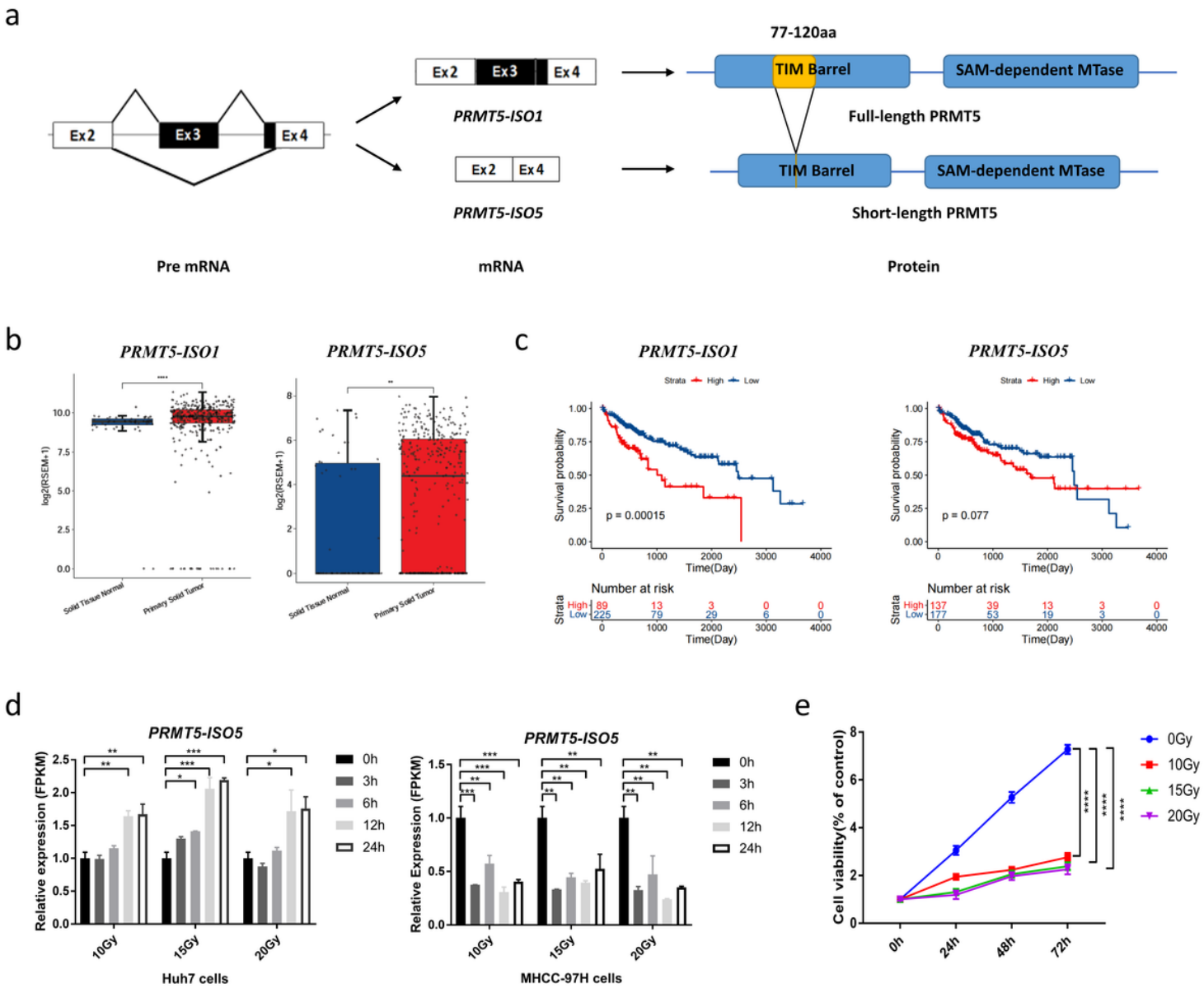

Figure 1

Radiation-induced *PRMT5-ISO5* production inhibits cell proliferation and improves the poor prognosis of HCC. (a) The splicing variant *PRMT5-ISO5* skips exon 3 and part of exon 4 of *PRMT5* and forms the shorter protein. (b) The transcriptional levels of *PRMT5* splicing variants associated with HCC were analyzed using Kruskal-Wallis test. $^{**}P < 0.01$, $^{****}P < 0.0001$. (c) The Kaplan-Meier Curves of overall survival were analyzed using Log-Rank Tests. The patients' datasets were from TSVdb TCGA Splicing Variants Database (http://www.tsvdb.com/plot.html). (d) The different change of *PRMT5-ISO5* induced by IR was detected by RT-qPCR. $^{*}P < 0.05$, $^{**}P < 0.01$, $^{***}P < 0.001$. (e) The cell proliferation of Huh7 cells was detected after IR treatment. $^{****}P < 0.0001$.

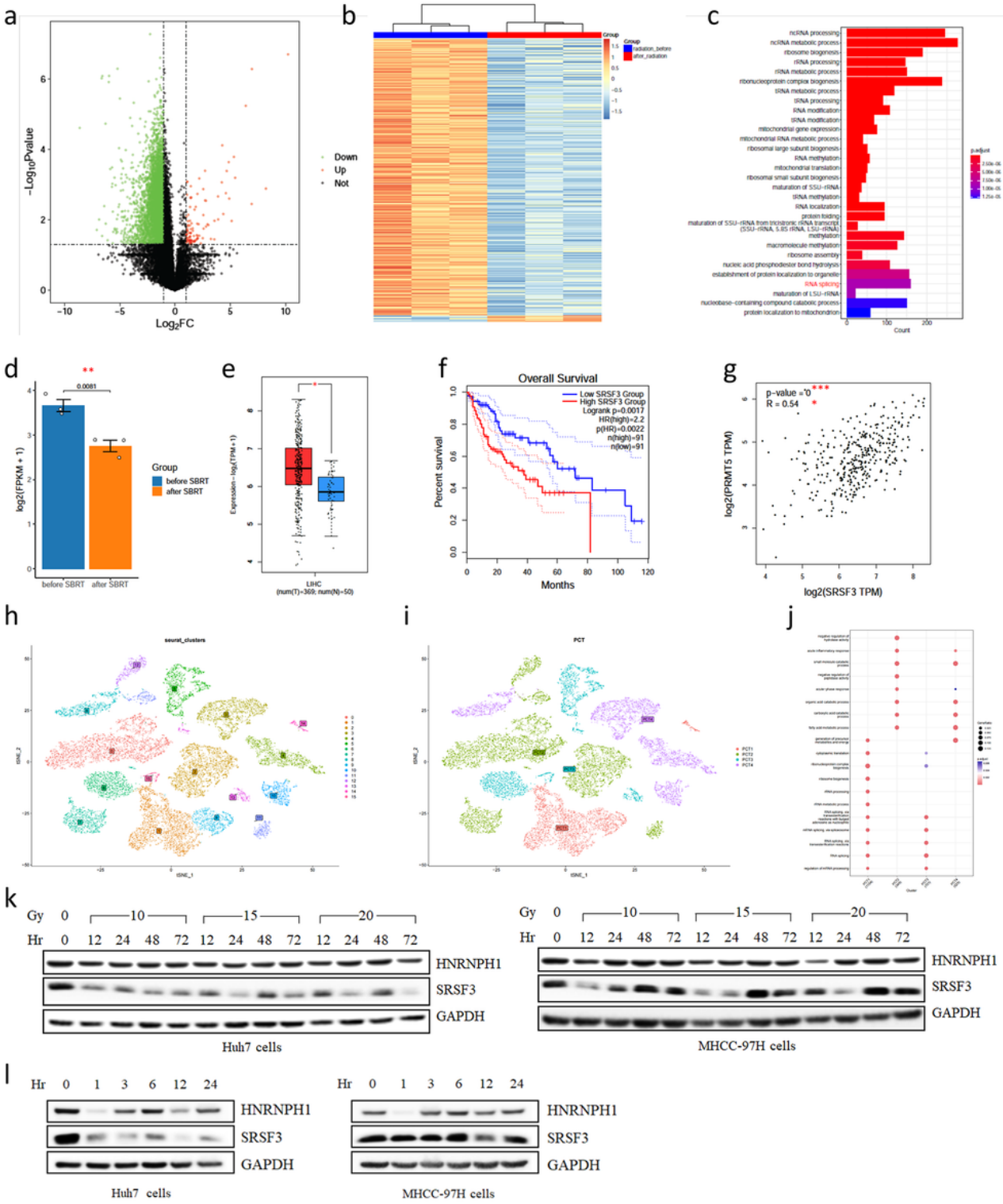

Figure 2

IR-induced *PRMT5-ISO5* production is regulated by SRSF3 and HNRNPH1 in HCC cells. (a) Significantly differential expression of genes was exhibited in volcano plot. (b) Clustering analysis was shown in Heatmap. (c) Go analysis was performed and top 30 pathway enrichment was revealed by bar charts. (d) The expression change of SRSF3 in HCC patients who received SBRT, (e) differential expression and (f) overall survival of SRSF3 in LIHC and normal control, (g) correlation of SRSF3 and PRMT5 were analyzed

separately. $^{*}P < 0.05$, $^{**}P < 0.01$, $^{****}P < 0.0001$. (h) t-SNE of the 15 cell clusters and (i) 4 cell populations from scRNA-seq datasets (GSE149614). (j) The GO analysis of 4 cell populations. (k-l) The expression change of SRSF3 and HNRNPH1 post-IR treatment was detected at different time points.

Figure 3

SRSF3 and HNRNPH1 play opposite roles in *PRMT5-ISO5* production induced by IR. (a) The efficiencies of si-*HNRNPH1* and si-*SRSF3* were detected by western blotting both in Huh7 and MHCC-97H cells (H1/2: si-*HNRNPH1*-1/2, S1/2: si-*SRSF3*-1/2, N: nonsense siRNA). (b) The level change of *PRMT5-ISO5* induced by HNRNPH1 silencing or SRSF3 depletion was detected (siH1-1/2: si-*HNRNPH1*-1/2, siS3-1/2: si-*SRSF3*-1/2,siNC: nonsense siRNA). $^{**}P < 0.01$. (c) HNRNPH1 or SRSF3 interference accompanied with IR treatment influenced the level of *PRMT5-ISO5* both in Huh7 cells, (d) MHCC-97H cells, (e) $PRMT5^{minigene}$ Huh7 cells, and (f) $PRMT5^{minigene}$ MHCC-97H cells (siH1: si-*HNRNPH1*, siS3: si-*SRSF3*, siNC: nonsense siRNA, $PRMT5^{minigene}$:PRMT5 KO clones transfected with *PRMT5-minigene* construct). $^{*}P < 0.05$, $^{**}P < 0.01$, $^{***}P < 0.001$, $^{****}P < 0.0001$.

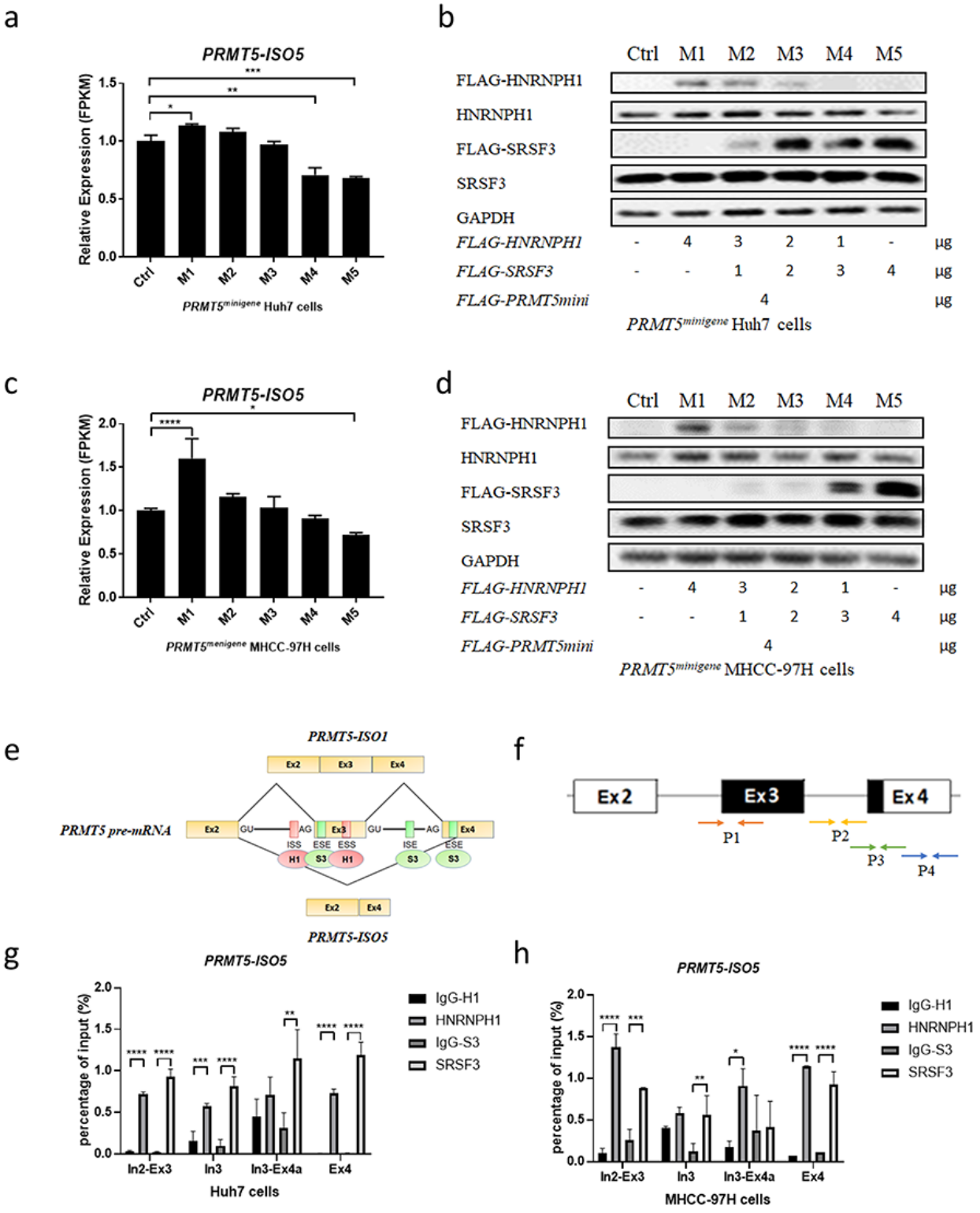

Figure 4

SRSF3 and HNRNPH1 competitively bind with *PRMT5* pre-mRNA and regulate *PRMT5* splicing. (a, c) The level change of *PRMT5-ISO5* and (b, d) endo- and exogenous expression of HNRNPH1/SRSF3 (Ctrl: 4 μg pcDNA3.1-*FLAG* vector, M1-5: 4, 3, 2, 1, 0 μg pcDNA3.1-*FLAG-HNRNPH1* mixed with 0, 1, 2, 3, 4 μg pcDNA3.1-*FLAG-SRSF3*) in *PRMT5*^{minigene} Huh7 cells and *PRMT5*^{minigene} MHCC-97H cells. FLAG-HNRNPH1 and FLAG-SRSF3 fusion proteins were detected with anti-FLAG, while HNRNPH1, SRSF3, and

GAPDH were determined using target antibodies. $^{*}P < 0.05$, $^{**}P < 0.01$, $^{***}P < 0.001$, $^{****}P < 0.0001$. (e) The potential binding region of HNRNPH1/SRSF3 in *PRMT5* pre-mRNA. (f) The primers targeted to the potential binding region were designed for RIP-qPCR detection (P1: primers of pair 1 targeted to intron 2 and partial exon 3, P2: primers of pair 2 located in intron 3, P3: primers of pair 3 amplified for intron 3 and partial exon 4 (exon 4A), P4: primers of pair 4 targeted to exon 4). (g-h) SRSF3 and HNRNPH1 shared the homologous binding region in *PRMT5* pre-mRNA (In2: intron 2, Ex3: exon 3, In3: intron 3, Ex4a: partial exon 4 (exon 4A), Ex4: exon 4). IgG-H1 and HNRNPH1 were collected from HNRNPH1 overexpression cells, while IgG-S3 and SRSF3 were gained from cells transfected with pcDNA3.1-*FLAG-SRSF3* expression construct. Fold enrichment was determined after normalization to the input compared with IgG control. $^{*}P < 0.05$, $^{**}P < 0.01$, $^{***}P < 0.001$, $^{****}P < 0.0001$.

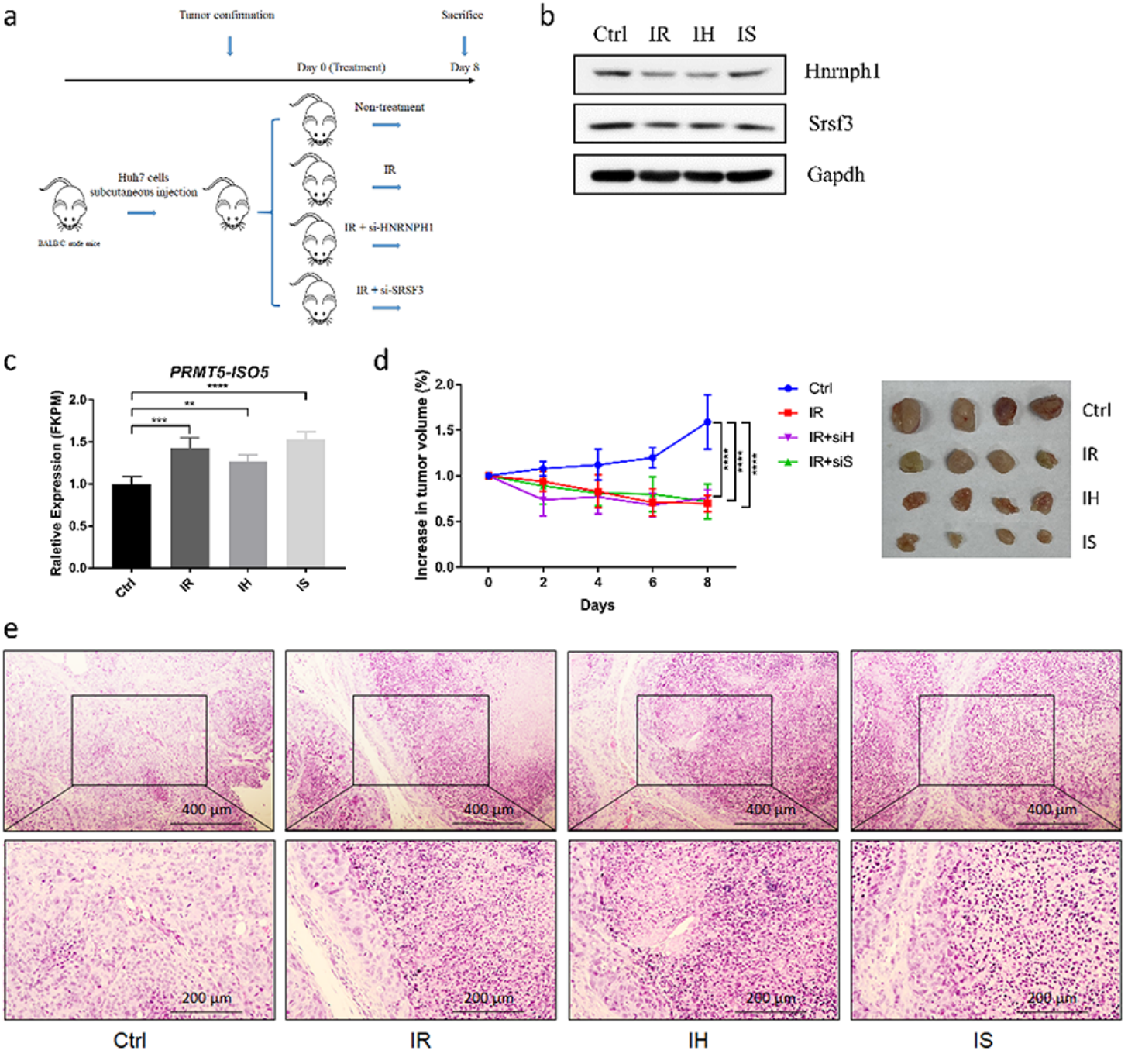

Figure 5

The increase of *PRMT5-ISO5* inhibits tumor growth in vivo. (a) The procedure of HCC xenograft model and treatments (n=4 for each group). (b) The efficiencies of IR treatment or accompanied with HNRNPH1/SRSF3 interference, compared with untreated-tumors from random volunteers. (c) The transcriptional change of *PRMT5-ISO5*, (d) tumor growth, and (e) representative images with H&E staining of tumor sections (200×) with IR or accompanied with siRNAs injection. Ctrl: tumors without further treatment, IR: tumors with IR treatment, IH: tumors with IR and in vivo si-HNRNPH1 intratumoral injection, IS: tumors with IR and in vivo si-SRSF3 intratumoral injection. $^{**}P < 0.01$, $^{***}P < 0.001$, $^{****}P < 0.0001$.

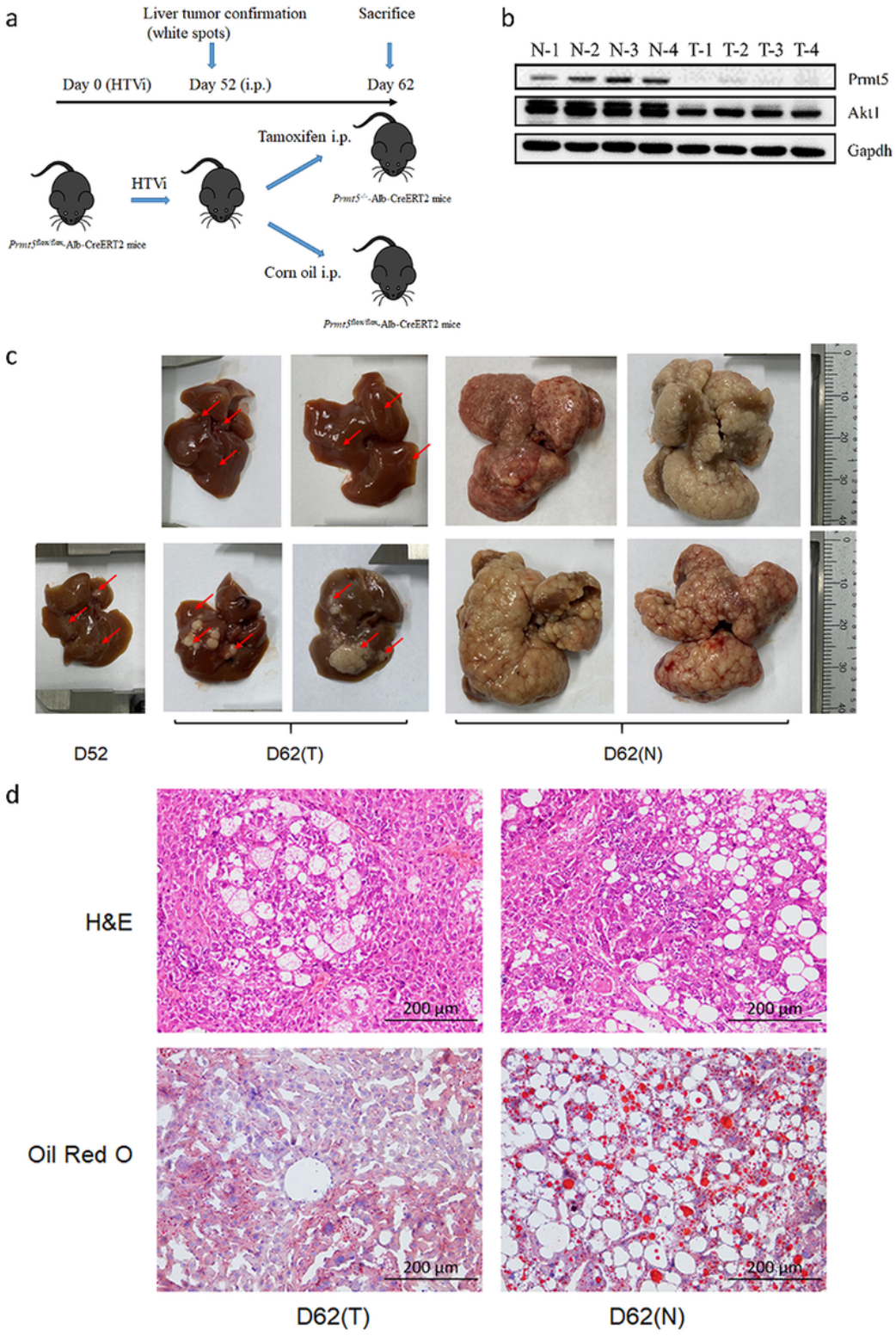

Figure 6

Prmt5 deficiency inhibits Akt/N-Ras-induced HCC progression. (a) The procedure of primary HCC model induced by overexpression of Akt1 and N-RasV12 using HTVi and liver specific KO treatment (i.p.: intraperitoneal injection). (b) Tamoxifen reduced the expression of Prmt5 in the liver (T-1/4: CKO group received tamoxifen injection, N1/4: non-CKO without tamoxifen injection). (c) Livers harvested from the mice at indicated time points after treatment. (White spots with red arrows represented spontaneous

lesions. D: days after HTVi treatment, T: *Prmt5* CKO group received tamoxifen intraperitoneal injection, N: non-CKO received corn oil intraperitoneal injection). (d) Representative liver images with H&E and Oil Red O staining of liver sections (200×).

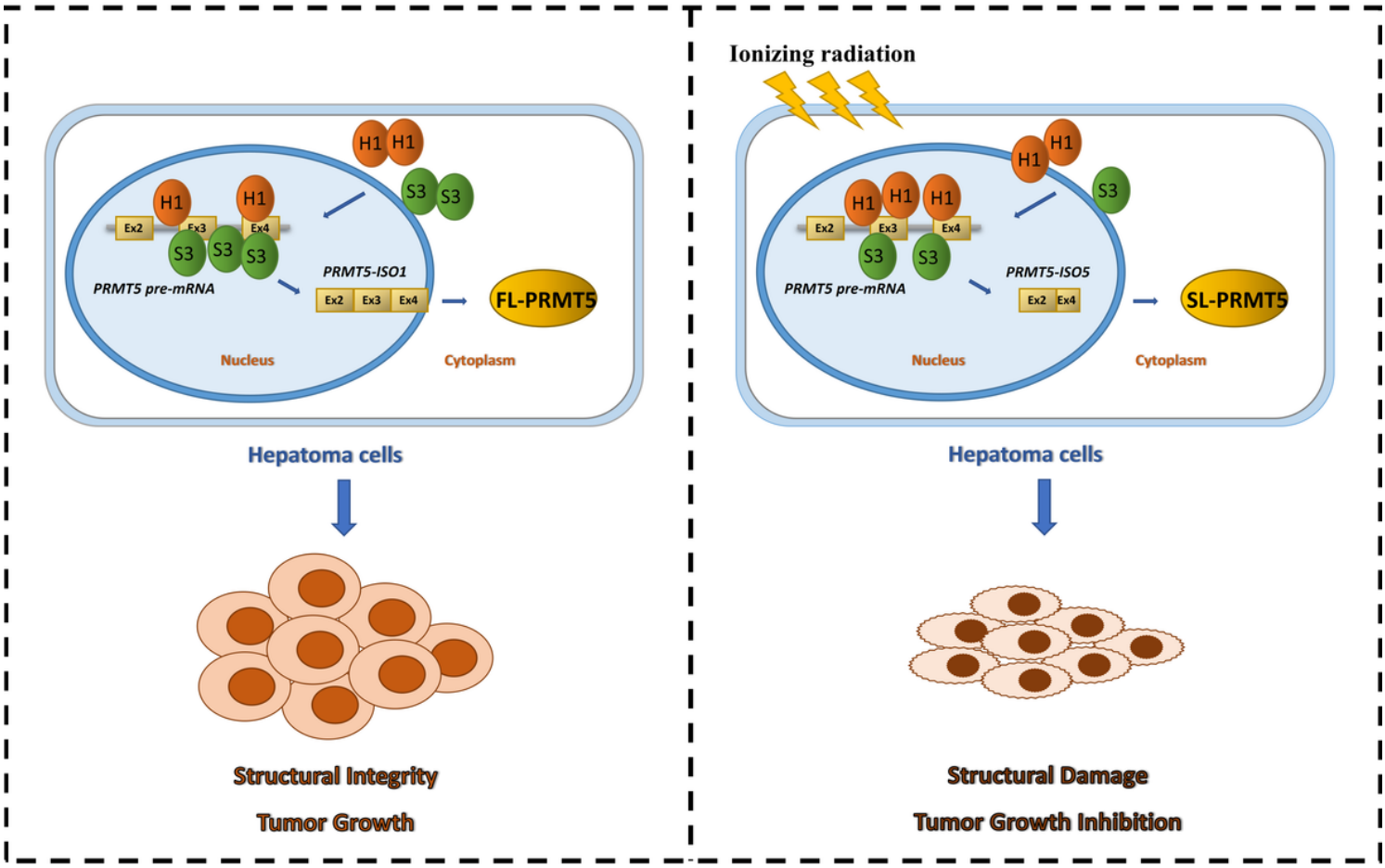

Figure 7

A schematic diagram illustrating SRSF3 and HNRNPH1 regulate *PRMT5-ISO5* transcript induced by IR in HCC. Normally, canonical *PRMT5-ISO1* is the main isoform which translates into full-length PRMT5 (FL-PRMT5) and promotes HCC development (left). Receiving IR treatment, SRSF3 (S3) and HNRNPH1 (H1) competitively binds to *PRMT5* pre-mRNA, leading to *PRMT5* exon 3 and partial exon 4 skipping. The increased *PRMT5-ISO5* translates into the shorter protein (SL-PRMT5) which promotes tumor regression of HCC (right).

Supplementary Files

This is a list of supplementary files associated with this preprint. Click to download.

- SupplementaryFig.S1.tif
- SupplementaryFig.S2.tif

- SupplementaryFig.S3.tif
- SupplementaryFig.S4.tif
- SupplementaryInformation.docx